Dispersion-Induced Beam Instability in Circular Accelerators

Y. S. Yuan,[1] O. Boine-Frankenheim,[1,2] G. Franchetti,[2] and I. Hofmann[1,2]
[1]Technische Universität Darmstadt, Schlossgartenstrasse 8, 64289 Darmstadt, Germany
[2]GSI Helmholtzzentrum für Schwerionenforschung GmbH, Planckstrasse 1, 64291 Darmstadt, Germany
(Received 11 October 2016; published 10 April 2017)

The envelope instability near the 90° phase advance in periodically focused space charge dominated beams is a well-known phenomenon in linear transport sections or linacs. The corresponding stop band is usually avoided because of the resulting strong mismatch oscillations and beam loss. We show that in circular accelerators or transport sections including bending magnets the instability is modified due to the effect of dispersion. Using the two-dimensional envelope equations extended by the dispersion equation we identify an additional stop band above 120°. For periodic focusing the stop band results from the confluence of an envelope mode with the newly identified coherent dispersion mode. Results from perturbation theory are compared with the full envelope model and particle-in-cell simulation, which all show good agreement. The newly identified mode has several implications and applications for the characterization of intense beams in circular machines.

DOI: 10.1103/PhysRevLett.118.154801

A detailed understanding of the physics of high-intensity proton or ion beams in linear and circular accelerators is of fundamental importance for many research areas, which rely on such beams, such as spallation neutrons sources or radioactive beam factories. In this context, studies of beam intensity limitation by space charge effects and measures to increase such space charge limits are of essential importance. Because of recent observations in high-intensity linear accelerators [1,2] the well-known 90° envelope instability [3] or second order parametric resonance [4] has received renewed interest, as it represents a major intensity limitation not only in linacs, but also in circular machines. In the past few years fruitful work has been initiated on this subject, for example, in Refs. [5–15]. The situation in circular accelerators for high-intensity beams is further complicated due to the presence of dispersion. Recent projects [16,17] require circular accelerators to accumulate high beam intensity; hence, the study of dispersion induced effects has received more attention. Progress has been made in understanding the combined effect of space charge and dispersion on beam dynamics. For matched two-dimensional beams Venturini and Reiser (V-R) [18,19] developed an envelope model with a generalized invariant emittance in the presence of both dispersion and space charge. Another approach by Lee and Okamoto (L-O) [20] resulted in a space charge modified equation for the dispersion. Both approaches indicate that in the presence of linear space charge forces and dispersion, a matched particle distribution exists. Other studies related to dispersion are performed within the smooth approximation approach [21] and the modified particle-core model [22–24]. In the later study, Ikegami introduced stable dispersion modes, which provide some insight into the role of dispersion for coherent beam oscillations. Note that previous studies assumed stable beams and did not consider the role of dispersion on the stability of high intensity beams. So far the theoretical framework of (transverse) beam envelope instabilities has been developed mainly for linear accelerators.

In this Letter, we report a new phenomenon in intense beams in circular accelerators, namely, the dispersion-induced beam instability, which is characterized by a resonance between the second order even mode (envelope mode) and a coherent dispersion mode described here.

In the following we assume x and y are the transverse degrees in the horizontal and vertical direction, respectively, s the longitudinal coordinate, and $k_{0,x,y}$, $k_{x,y}$ are the phase advance per focusing cell without and with space charge, respectively. Consider a coasting beam in a periodic focusing structure with bending magnets. The Hamiltonian of the system is

$$H = \frac{1}{2}(p_x^2 + p_y^2) + \frac{\kappa_{x0}(s)}{2}x^2 + \frac{\kappa_{y0}(s)}{2}y^2 + \frac{m^2c^4}{E_0^2}\delta^2 - \frac{x}{\rho(s)}\delta + V_{sc}(x, y, s), \quad (1)$$

where $\kappa_{x0}(s)$, $\kappa_{y0}(s)$ are the focusing gradients, $\rho(s)$ the radius of curvature, and $\delta = (p - p_0)/p_0$ the fractional momentum deviation from the design momentum p_0 with E_0 being the corresponding energy and V_{sc} the space charge potential. With canonical transformation introduced in the V-R and L-O frameworks: $x = \bar{x} + \delta D_x$, $p_x = \bar{p}_x + \delta D_x'$, $y = \bar{y}$, $p_y = \bar{p}_y$, we introduce $\bar{x}$ and $\bar{p}_x$ as the betatron coordinates affected by space charge, and $D_x\delta$, $D_x'\delta$ the off-momentum coordinate affected by space charge. The coefficients D_x and D_x' will eventually be identified with the space-charge-modified dispersion and

its derivative. Following Sacherer's approach [25] we obtain,

$$\left\langle x\frac{\partial V_{sc}}{\partial x}\right\rangle = \frac{K_{sc}}{2X(X+Y)}(\sigma_x^2+\sigma_\delta^2 D_x^2), \tag{2}$$

in which $\langle\cdot\rangle$ denotes the averaging over phase space variables; $\sigma_x=\sqrt{\langle\bar{x}^2\rangle}$, $\sigma_y=Y=\sqrt{\langle y^2\rangle}=\sqrt{\langle\bar{y}^2\rangle}$, $\sigma_\delta=\langle\delta^2\rangle$, $X=\sqrt{\langle x^2\rangle}=\sqrt{\sigma_x^2+\sigma_\delta^2 D_x^2}$, and K_{sc} the space charge perveance parameter, defined by $K_{sc}=2N_L r_c/(\beta^2\gamma^3)$, with N_L the number of particles per length, r_c the classical proton radius, β and γ the relativistic factors. Equation (2) shows that beam motion can be expressed as a linear superposition of the betatron oscillations and dispersion, independent of the form of particle distribution.

The space-charge-modified dispersion function can be defined from Eq. (1) and Eq. (2):

$$\frac{d^2D_x}{ds^2}+\left(\kappa_{x0}(s)-\frac{K_{sc}}{2X(X+Y)}\right)D_x=\frac{1}{\rho(s)}, \tag{3}$$

with the corresponding rms envelope equations

$$\begin{aligned}\frac{d^2\sigma_x}{ds^2}+\left[\kappa_{x0}(s)-\frac{K_{sc}}{2X(X+Y)}\right]\sigma_x-\frac{\varepsilon_x^2}{\sigma_x^3}=0,\\ \frac{d^2\sigma_y}{ds^2}+\left[\kappa_{y0}(s)-\frac{K_{sc}}{2Y(X+Y)}\right]\sigma_y-\frac{\varepsilon_y^2}{\sigma_y^3}=0,\end{aligned} \tag{4}$$

where $\varepsilon_x=\sqrt{\langle\bar{x}^2\rangle\langle\bar{p}_x^2\rangle-\langle\bar{x}\bar{p}_x\rangle^2}$ (similar in ε_y) is the generalized rms emittance. Since the beam envelope $X(s)$ contains two independent contributions: $\sigma_\delta D_x(s)$ and $\sigma_x(s)$, it is convenient to introduce a "dispersion ratio" $\cos\theta$, and the corresponding "betatron ratio" $\sin\theta$ to estimate the extent of the beam motion being affected by dispersion, defined by $\cos\theta=\sigma_\delta D_x(s)/X(s)$ and $\sin\theta=\sigma_x(s)/X(s)$ $(0<\theta<\pi/2)$, respectively. Clearly, a larger dispersion ratio means a larger dispersion effect.

For periodic $\kappa_{x0}(s)$, $\kappa_{y0}(s)$, and $\rho(s)$, matched solutions $\{\sigma_{x0},\sigma_{y0},D_{x0}\}$ can be obtained from Eq. (3) and Eqs. (4). Let us assume a slightly mismatched envelope with $\{\sigma_x,\sigma_y,D_x\}$ and small perturbations $\{\xi,\eta,d_x\}$: $\sigma_x=\sigma_{x0}+\xi$, $\sigma_y=\sigma_{y0}+\eta$ and $D_x=D_{x0}+d_x$. After neglecting the higher order terms and introducing the horizontal beam width $X=X_0+\xi\sigma_{x0}/X_0+\sigma_\delta^2 D_{x0}d_x/X_0$, we can obtain from Eq. (3) and Eqs. (4) the envelope oscillation system, which can be written in a matrix form:

$$\frac{d^2}{ds^2}\begin{pmatrix}\xi\\ \eta\\ d_x\end{pmatrix}=\begin{pmatrix}-a_0 & -a_1 & -a_2\\ -a_1 & -a_3 & -a_4\\ -\frac{a_2}{\sigma_\delta^2} & -\frac{a_4}{\sigma_\delta^2} & -a_5\end{pmatrix}\begin{pmatrix}\xi\\ \eta\\ d_x\end{pmatrix}, \tag{5}$$

and

$$\begin{aligned}a_0&=4\kappa_x-\frac{2r+1}{r+1}\Delta\kappa_x\sin^2\theta_0, \quad a_1=\frac{r}{r+1}\Delta\kappa_x\sin\theta_0,\\ a_2&=\frac{2r+1}{r+1}\sigma_\delta\Delta\kappa_x\sin\theta_0\cos\theta_0, \quad a_3=4\kappa_y+\frac{r+2}{r+1}\Delta\kappa_y,\\ a_4&=\frac{r}{r+1}\sigma_\delta\Delta\kappa_x\cos\theta_0, \quad a_5=\kappa_x+\frac{2r+1}{r+1}\Delta\kappa_x\cos^2\theta_0.\end{aligned}$$

Here we use the following notation: beam size ratio $r=X_0/Y_0$; dispersion ratio for matched case: $\cos\theta_0=\sigma_{\delta0}/X_0$, betatron ratio for matched case: $\sin\theta_0=\sigma_{x0}/X_0$; space charge modified focusing gradients $\kappa_x=\kappa_{x0}-\Delta\kappa_x$ and $\kappa_y=\kappa_{y0}-\Delta\kappa_y$, where $\Delta\kappa_x=K_{sc}/[2X_0(X_0+Y_0)]$ and $\Delta\kappa_y=K_{sc}/[2Y_0(X_0+Y_0)]$ are the space charge induced shifts. Equations (5), recognized as a set of second order differential equations behaving like three coupled harmonic oscillators, can be decoupled to three fundamental modes with oscillation frequencies $\{\omega_i\}$ and the corresponding phase shift $\{\phi_i=2\pi\omega_i\}$ $(i=1,2,3)$. For periodic focusing algebraic expressions for the fundamental modes require numerical methods since κ_{x0}, κ_{y0}, κ_x and κ_y are functions of s.

For constant focusing with $\kappa_{x0}(s)=\kappa_{y0}(s)=\kappa_0$, $\rho(s)=\rho_0$, and $k_{0,x}=k_{0,y}=k_0$, solutions can be found which can provide useful physical insight: in the limit of zero beam current Eqs. (5) are decoupled and the phase shifts of three fundamental modes are

$$\phi_1=\phi_2=2k_0, \qquad \phi_3=k_0. \tag{6}$$

On the other hand, for strong space charge, approaching the space charge limit, we have,

$$\phi_1=k_0, \qquad \phi_2=\sqrt{2}k_0, \qquad \phi_3=0. \tag{7}$$

In both limits, ϕ_1 and ϕ_2 have the identical form as in the case without dispersion: quadrupole (slow) mode, breathing (fast) mode; the additional mode, which is related to dispersion, behaves differently and its phase shift ϕ_3 tends to be zero in the space charge limit.

A generalized stability analysis can be performed by integrating Eqs. (5) over one focusing cell (from m to $m+1$)

$$\zeta_{m+1}=M\zeta_m, \tag{8}$$

where M is the map for the perturbation vector $\zeta=(\xi,\xi',\eta,\eta',d_x,d_x')$ over one cell. As $\{\sigma_x,\sigma_x',\sigma_y,\sigma_y',D_x,D_x'\}$ in Eq. (3) and Eqs. (4) follow a Hamiltonian, the six eigenvalues of M: $\lambda_i=|\lambda_i|e^{i\phi_i}(i=1,2,\ldots,6)$ exist only as reciprocal or as conjugate in three pairs: $\{\lambda_1,\lambda_1^*\}$, $\{\lambda_2,\lambda_2^*\}$, $\{\lambda_3,\lambda_3^*\}$. Moreover, taking each oscillation mode in space charge limits as reference, we can select a suitable set of phase shifts $\{\phi_1,\phi_2,\phi_3\}$ with corresponding moduli $\{|\lambda_1|,|\lambda_2|,|\lambda_3|\}$ representing quadrupole mode, breathing

mode and the mode from dispersion oscillation, respectively, to fully characterize the beam oscillation system without loss of generality. One of three moduli larger than unity can be used as instability growth factor.

Let us analyze the beam stability using the example of a FODO cell with dipoles [26] formed by the sequence: $\{\frac{1}{2}\mathrm{QF\,B\,QD\,B}\,\frac{1}{2}\mathrm{QF}\}$, in which QF and QD denote focusing and defocusing quadrupoles, respectively, and B represents dipoles acting along x. For simplicity, we chose $k_{0,x} = k_{0,y} = k_0$. To make the example more representative, lattice, dispersion functions, and rms momentum spread are chosen such that the dispersion effect is close to existing circular accelerators: in our FODO example, the maximum of the dispersion ratio for zero current is $\cos\hat{\theta}_0 = 0.4$, while in existing circular accelerators $0.35 < \cos\hat{\theta}_0 < 0.6$ for typical reference parameters. Consider a continuous beam with finite rms momentum spread and identical emittances in x and y. The numerical integration of Eq. (8) is performed and the results for $\{\phi_1, \phi_2, \phi_3\}$ together with the growth factor versus beam current are obtained and shown for two representative cases: $k_0 = 120°$ and 130°, as shown in Figs. 1 and 2. For a more illustrative analysis of the dispersion-induced instability, we introduce another notation to represent the phase shift of dispersion oscillation mode, namely, the coherent dispersion mode: $\phi_d = 360° - \phi_3$. As can be seen in Fig. 1, ϕ_1, ϕ_2 decrease from $2k_0$ and ϕ_3 decreases from k_0, while ϕ_d increases from $360° - k_0$, which is in agreement with the conclusion of Eq. (6). Note that the well-known 90° envelope instability, i.e., parametric resonance and confluent resonance occurs from $k_x = 92°$. No confluence exists between ϕ_d and ϕ_1 or ϕ_2.

The appearance of the dispersion-induced instability is shown in Fig. 2 for $k_0 = 130°$. The growth factor region (stop band) from $k_x = 118°$ to 110° indicates instability (the simulation results for the emittance growth and phase space evaluation shown in Fig. 2 will be discussed later). Since in the region of $k_x = 118°$ to 110°, confluence occurs between the dispersion mode ϕ_d and the slow mode ϕ_1, this instability is induced by periodic focusing and dispersion and can be related to a resonance between these two modes.

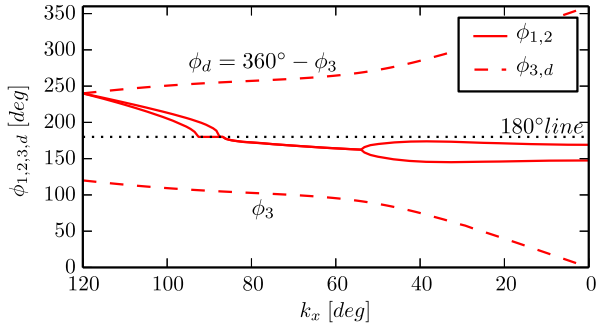

FIG. 1. $k_0 = 120°$ case: Phase shifts ϕ_1, ϕ_2 (solid line) and ϕ_3, ϕ_d (dashed line) versus depressed phase advance k_x with dispersion.

Besides, parametric and confluent resonances exist below $k_x = 94°$. A criterion for the occurrence of dispersion-induced instability can be given based on the following analyses: in Fig. 2, $\phi_1^0 = 260°$, $\phi_d^0 = 240°$, and $\phi_d^0 < \phi_1^0$ (here the superscript "0" denotes values in the absence of space charge). This is different from the case in Fig. 1, in which $\phi_1^0 = \phi_2^0 = \phi_d^0 = 240°$ and no confluence occurs between ϕ_1 and ϕ_d. These analyses show that only if $\phi_1^0 > \phi_d^0$, e.g., $2k_0 > 360° - k_0$, or $k_0 > 120°$, ϕ_1 and ϕ_d can be confluent, and, hence, the dispersion-induced instability occurs. In other words, for a lattice of $k_{0,x} = k_{0,y} = k_0$, only with $k_0 > 120°$ satisfied, the dispersion-induced instability may occur within a certain beam current range. For a more physical interpretation, the extended envelope oscillation system including dispersion contains three fundamental modes. The mode of dispersion oscillation (ϕ_d or ϕ_3) behaves, to some extent, like a single particle as Eq. (3) lacks the emittance term, which is different from the two other modes ϕ_1 and ϕ_2. For a lattice of $k_{0,x} = k_{0,y} = k_0$ only with $k_0 > 120°$, ϕ_d mode may resonate with ϕ_1 mode in a certain beam current range, and induce the beam instability with the periodic focusing.

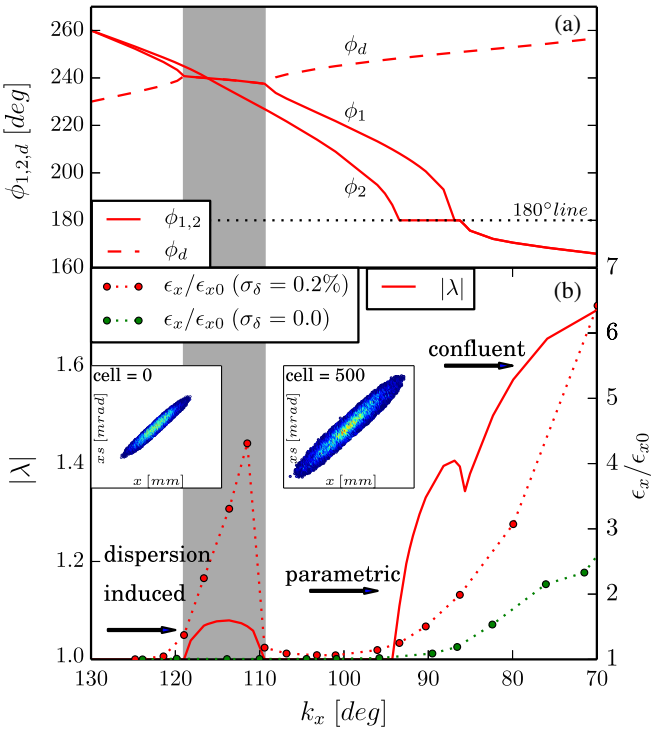

FIG. 2. $k_0 = 130°$ case: (a) Phase shifts ϕ_1, ϕ_2 (solid line) and ϕ_d (dashed line) versus depressed phase advance k_x with dispersion and (b) growth factor $|\lambda|$ (solid line) from numerical calculation and normalized emittance growth ϵ_x/ϵ_{x0} (dotted line) from PIC simulation versus depressed phase advance k_x with and without dispersion. (Shaded area denotes the stop band of the dispersion-induced instability.) Insets: $x - x'$ phase space distribution at 0 and 500 periodic cell.

The criteria above can be extended to a more general case. Let us consider a periodic lattice with $k_{0,x} > k_{0,y}$. With increasing beam current the slow mode ϕ_1 and the fast mode ϕ_2 decrease from $2k_{0,y}$ and $2k_{0,x}$ respectively, while ϕ_d increases from $360° - k_{0,x}$. Therefore, ϕ_2 can be confluent with ϕ_d when satisfying $2k_{0,x} > 360° - k_{0,x}$, e.g.,

$$k_{0,x} > 120°. \tag{9}$$

Therefore, the dispersion-induced envelope instability can be named "120° dispersion instability," in contrast to the usual envelope instability related to $k_{0,x,y} > 90°$.

Some main features of the 120° dispersion instability are discussed as follows. Since $\phi_d = 360° - \phi_3$, the condition $\phi_{1,2} = \phi_d$ is actually $\phi_{1,2} + \phi_3 = 360°$. Therefore, the dispersion-induced instability can be identified as a "sum parametric resonance" [15] between the envelope mode ϕ_1 or ϕ_2 and the dispersion mode ϕ_3. An interesting question may be raised as to whether the dispersion mode ϕ_d (or ϕ_3) can resonate with the lattice by itself, just like the well-known parametric resonance characterized by ϕ_1 mode or ϕ_2 mode locked to the 180° line. The main point is that typically for a basic focusing cell $k_{0,x,y}$ is smaller than 180°, which means ϕ_d is always larger than 180° or ϕ_3 is always smaller than 180°. Consequently, ϕ_d (or ϕ_3) will not reach the 180° line and resonate with the lattice.

For an overview of the appearance of dispersion-induced instability, a kind of envelope resonance diagram is calculated by solving the full envelope model of Eq. (3) and Eqs. (4), numerically. This is shown in Fig. 3 as a color-coded plot displaying the maximum envelope mismatch factors achieved over 200 cells versus $k_{0,x}$ and $k_{0,y}$ as variables. The mismatch factor measures the deviation of the envelopes from their initially matched values following Ref. [27]. Both the beam current and rms momentum spread are held at a fixed value (in our example, $k_x - k_{0,x} \approx -15°$, $\sigma_\delta = 0.2\%$). The vertical and horizontal bands around $k_{0,x} = 100°$ and $k_{0,y} = 100°$ represent the conventional 90° envelope instabilities; the thin diagonal with negative slope denotes the sum envelope instability [15]. In comparison, an additional vertical band appears around $k_{0,x} = 130°$. This band represent the 120° dispersion-induced instability.

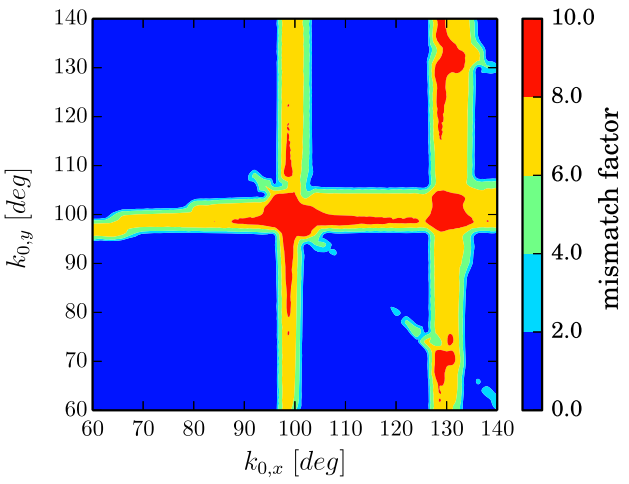

FIG. 3. Scan of the mismatch factor (color coding) from the full envelope equations with dispersion after 200 cells.

PIC simulations have been performed using PyORBIT [28] to support the above results and conclusions from both, the envelope oscillation theory in Fig. 2 and the full envelope model in Fig. 3. The initial particle distribution is chosen as a transverse waterbag, which is rms matched using the stationary solutions obtained from the envelope model. In the simulation, the horizontal emittance growth (normalized to initial one) ϵ_x/ϵ_{x0} is taken after 500 focusing periods, at which time both the beam size and emittance growth caused by envelope instability have already saturated. As shown in Fig. 2(b) by the dotted line curve, an emittance growth is only observed with nonzero beam momentum spread in the range of $k_x = 118°$ to 110° and in agreement with the corresponding region of the growth factor $|\lambda|$ from the envelope oscillation theory. This is a clear validation of the dispersion-induced instability, since neither the usual 90° envelope instability nor the fourth order structure resonance [6,13,29] exist within this region. The corresponding simulation results for the particle distribution are shown in the insets: with the initial distribution at $k_x = 115°$, notable emittance growth can be observed after 500 periodic cells. It is worth pointing out that the profile of emittance growth in Fig. 2(b) is "sawtooth," with one sharper side of emittance growth rate at $k_x = 110°$, which differs significantly from the "rounded" profile for the growth factor. We interpret this similar to the case of the 90° instability [6,13]. Within the stop band of the 120° dispersion instability the beam tends to reach a stable state by self-detuning due to the accompanying emittance growth, until it leaves the stop band. Since the detuning process occurs always in the direction of weaker space charge, the beam has to go through the whole range of the stop band with larger emittance growth, if crossing from the side of $k_x = 110°$. In comparison, the growth factor, which is numerically obtained by integration of Eq. (8) [solid line curve in Fig. 2(b)], lacks the information on the beam self-detuning process, since the envelope approach describes only the onset, rather than the saturation of the instability. A further examination shows that the emittance growth, the eigenvalues in Fig. 2, and the mismatch factor in Fig. 3, which all characterize the dispersion instability, are in agreement in the range of the 120° dispersion instability, in terms of the beam current. For example, the points $k_{x,0} = 130°$, $k_{y,0} = 130°$ in Fig. 3 are in accordance with the point $k_x = 115°$ in Fig. 2, both of which are located in the stop band.

In summary, we have shown that in the presence of dispersion and space charge a coherent dispersion mode

exists, besides the well-known slow and fast envelope modes. This dispersion mode has been identified within a generalized envelope oscillation model and full numerical solutions of a set of envelope equations, including dispersion, as well as in PIC simulations. For phase advances larger than 120° and lattice parameters similar to modern high-intensity synchrotrons, we find that the dispersion mode is unstable. Our analysis reveals that this dispersion-induced instability in periodic focusing lattices is characterized by the confluence of the fast mode or slow envelope mode (i.e., the second-order even mode) with the dispersion mode.

We expect that the coherent dispersion mode and its instability will have implications for the choice of the working point in high intensity circular accelerators. An important application would be the experimental identification of the space charge modified dispersion mode from the transverse beam spectra: The observation of the dispersion mode could be a method to dynamically characterize the space-charge-modified dispersion. Measurements in circular accelerators could take advantage of quadrupolar pickup signals to identify the envelope modes [30,31] and the new coherent dispersion mode, which would give a full dynamical characterization of the relevant optical functions modified by space charge. Furthermore, the identified 120° stop band could be avoided during bunch compression [32–34] in synchrotrons and might play a role in ERLs and recirculators.

Our results could trigger further studies of confluence with other modes [4,35,36]. Furthermore, the role of synchrotron motion on this new instability in bunched beams deserves additional study.

The authors would like to thank Dr. J. Struckmeier (GSI) for discussions. One of the authors (Y. S. Yuan) was supported through a grant from HGS-HIRe for FAIR.

[1] L. Groening, W. Barth, W. Bayer, G. Clemente, L. Dahl, P. Forck, P. Gerhard, I. Hofmann, M. S. Kaiser, M. Maier, S. Mickat, T. Milosic, D. Jeon, and D. Uriot, Phys. Rev. Lett. **102**, 234801 (2009).
[2] L. Groening, I. Hofmann, W. Barth, W. Bayer, G. Clemente, L. Dahl, P. Forck, P. Gerhard, M. S. Kaiser, M. Maier, S. Mickat, T. Milosic, S. Yaramyshev, and D. Uriot, Phys. Rev. Lett. **103**, 224801 (2009).
[3] J. Struckmeier and M. Reiser, Part. Accel. **14**, 227 (1984); PARMILA code: http://laacg.lanl.gov/laacg/services/download_PMI.phtml.
[4] I. Hofmann, L. J. Laslett, L. Smith, and I. Haber, Part. Accel. **13**, 145 (1983); I. Hofmann, Phys. Rev. E **57**, 4713 (1998).
[5] C. Chen and R. C. Davidson, Phys. Rev. Lett. **72**, 2195 (1994).
[6] I. Hofmann and O. Boine-Frankenheim, Phys. Rev. Lett. **115**, 204802 (2015).
[7] S. Y. Lee and A. Riabko, Phys. Rev. E **51**, 1609 (1995).
[8] A. V. Fedotov and I. Hofmann, Phys. Rev. ST Accel. Beams **5**, 024202 (2002).
[9] B. L. Qian, J. Zhou, and C. Chen, Phys. Rev. ST Accel. Beams **6**, 014201 (2003).
[10] S. M. Lund and B. Bukh, Phys. Rev. ST Accel. Beams **7**, 024801 (2004).
[11] S. M. Lund, S. H. Chilton, and E. P. Lee, Phys. Rev. ST Accel. Beams **9**, 064201 (2006).
[12] A. Burov, Phys. Rev. ST Accel. Beams **9**, 120101 (2006).
[13] C. Li and Y. L. Zhao, Phys. Rev. ST Accel. Beams **17**, 124202 (2014).
[14] H. C. Chao and S. Y. Lee, Phys. Rev. ST Accel. Beams **18**, 024202 (2015).
[15] O. Boine-Frankenheim, I. Hofmann, and J. Struckmeier, Phys. Plasmas **23**, 090705 (2016).
[16] O. Kester, P. Spiller, and H. Stoecker, in *Challenges and Goals for Accelerators in the XXI Century*, edited by O. Brüning and S. Myers (World Scientific, Singapore, 2016), p. 611
[17] https://espace.cern.ch/liu-project.
[18] M. Venturini and M. Reiser, Phys. Rev. E **57**, 4725 (1998).
[19] M. Venturini and M. Reiser, Phys. Rev. Lett. **81**, 96 (1998).
[20] S. Y. Lee and H. Okamoto, Phys. Rev. Lett. **80**, 5133 (1998).
[21] S. Bernal, B. Beaudoin, T. Koeth, and P. G. O'Shea, Phys. Rev. ST Accel. Beams **14**, 104202 (2011).
[22] J. A. Holmes, V. V. Danilov, J. D. Galambos, D. Jeon, and D. K. Olsen, Phys. Rev. ST Accel. Beams **2**, 114202 (1999).
[23] M. Ikegami, S. Machida, and T. Uesugi, Phys. Rev. ST Accel. Beams **2**, 124201 (1999).
[24] S. Cousineau, S. Y. Lee, J. A. Holmes, V. Danilov, and A. Fedotov, Phys. Rev. ST Accel. Beams **6**, 034205 (2003).
[25] F. J. Sacherer, IEEE Trans. Nucl. Sci. **18**, 1105 (1971).
[26] See, e.g., S. Y. Lee, *Accelerator Physics* 3rd ed. (World Scientific, Singapore, 2011).
[27] T. P. Wangler, *RF Linear Accelerators*, 2nd ed. (Wiley-VCH, New York, 2008).
[28] A. Shishlo, S. Cousineau, V. Danilov, J. Galambos, S. Henderson, J. Holmes, and M. Plum, in *Proceedings of the 2006 International Computational Accelerator Physics Conference* (Chamonix Mont-Blanc, France, 2006), p. 53, https://sourceforge.net/projects/py-orbit.
[29] D. Jeon, L. Groening, and G. Franchetti, Phys. Rev. ST Accel. Beams **12**, 054204 (2009).
[30] R. Bär, I. Hofmann, P. Moritz, and U. Oeftiger, Nucl. Instrum. Methods Phys. Res., Sect. A **415**, 460 (1998).
[31] R. Singh, O. Boine-Frankenheim, O. Chorniy, P. Forck, R. Haseitl, W. Kaufmann, P. Kowina, K. Lang, and T. Weiland, Phys. Rev. ST Accel. Beams **16**, 034201 (2013).
[32] G. Franchetti, I. Hofmann, and G. Rumolo, Phys. Rev. ST Accel. Beams **3**, 084201 (2000).
[33] K. M. Fung, M. Ball, C. M. Chu, B. Hamilton, S. Y. Lee, and K. Y. Ng, Phys. Rev. ST Accel. Beams **3**, 100101 (2000).
[34] Y. Zou, J. Tang, J. Chen, X. Li, and H. Sun, Phys. Rev. ST Accel. Beams **17**, 060101 (2014).
[35] G. Franchetti, I. Hofmann, and M. Aslaninejad, Phys. Rev. Lett. **94**, 194801 (2005).
[36] I. Hofmann, G. Franchetti, O. Boine-Frankenheim, J. Qiang, and R. D. Ryne, Phys. Rev. ST Accel. Beams **6**, 024202 (2003).